To cite this article: WU W T, GU N, PENG Z H, et al. Distributed time-varying formation control for unmanned surface vehicles guided by multiple leaders [J/OL]. Chinese Journal of Ship Research, 2020, 15(1). http://www.ship-research.com/EN/Y2020/V15/I1/21.

DOI: 10.19693/j.issn.1673-3185.01734

Distributed time-varying formation control for unmanned surface vehicles guided by multiple leaders

WU Wentao, GU Nan, PENG Zhouhua, LIU Lu, WANG Dan*

Marine Electrical Engineering College, Dalian Maritime University, Dalian 116026, China

Abstract: [**Objectives**] This paper investigates the distributed time-varying formation control of a swarm of under-actuated unmanned surface vehicles (USVs) guided by multiple leaders in the presence of complex model uncertainties and unknown ocean disturbances. [**Methods**] At the kinematic level, distributed time-varying formation guidance laws are designed on the basis of the containment method and path maneuvering principle; at the kinetic level, the surge speed and yaw rate control laws are developed on the basis of the extended state observer (ESO) method such that the influences of the model uncertainties and unknown disturbances are mitigated. Further, cascade system stability analysis is undertaken, and the validity of the controller is demonstrated via a simulation. [**Results**] It shows that the closed-loop distributed time-varying formation control system for USV is input-to-state stable by the cascade system stability theory. The simulation results verify the effectiveness of the control method. [**Conclusions**] With the proposed controller, USVs are able to achieve the predefined time-varying formation while following the convex combination of multiple leaders.

Key words: under-actuated unmanned surface vehicle (USV); guidance and control law; time-varying formation control; multiple leaders; extended state observer (ESO)

CLC number: U674.91

0 Introduction

In recent years, with the rapid improvement of communication technology and embedded system performance, the development of intelligent devices such as an unmanned surface vehicle (USV), unmanned aerial vehicle (UAV), and mobile robot (MR) has been promoted. As an emerging type of unmanned surface platform, USV has been studied extensively [1-5]. So far, a single USV has been able to accomplish such tasks as target and path tracking and obstacle avoidance, but in the face of complex sea conditions, especially in the implementation of tasks such as military, rescue, and detection of fish school, higher requirements are put forward for the operational efficiency and speed of USV. The capability and efficiency of a single USV are generally difficult to meet the needs [6-9], and multiple USVs or clusters are required to jointly perform specific operational tasks. Therefore, in order to make the USV

Received: 2019-09-02 **Accepted:** 2019-11-25

Supported by: National Natural Science Foundation of China (61673081, 51979020); Support Program of Outstanding Young Scientific and Technological Talents of Dalian, Liaoning Province (2018RJ08)

Authors: WU Wentao, male, born in 1995, master degree candidate. Research interest: path control for USVs. E-mail: wuwentaodlmu@gmail.com

GU Nan, male, born in 1993, male, Ph.D. candidate. Research interest: control of USVs. E-mail: gunandlmu@gmail.com

PENG Zhouhua, male, born in 1982, Ph.D., professor, Ph.D. supervisor. Research interest: guidance and control of marine vehicles, and control of USVs. E-mail: zhpeng@dlmu.edu.cn

LIU Lu, male, born in 1990, Ph.D., lecturer, master's supervisor. Research interest: guidance and control of USVs, and cooperative control of multiple USVs. E-mail: luliu@dlmu.edu.cn

WANG Dan, male, born in 1960, Ph.D., professor, Ph.D. supervisor. Research interest: formation control of USVs and power electronic technology. E-mail: dwang@dlmu.edu.cn

***Corresponding author:** PENG Zhouhua

downloaded from www.ship-research.com

meet the higher application requirements, we need to develop the cooperative control of the USV formation and improve its intelligence level, which is of great significance [10-11].

At present, many control methods have been developed in the field of USV formation control, among which the representative ones are graph-theory-based method [12-13], virtual structure method [14], leader-following method [15] and artificial potential field method [16]. Among these methods, the graph-theory-based method has been deeply studied. According to the types of leaders, formation control methods can be divided into two types generally: One is cooperative control guided by tracks, and the other is cooperative control guided by paths. The latter has an outstanding advantage that spatial and temporal constraints can be decoupled [5,17]. In addition, a number of studies on distributed convergence and distributed formation control have been conducted on the issue of formation control. Based on the above studies, the formation can be determined by the formation tracking controller, with specific models including collision avoidance tracking of distributed formation, and leader following, etc. [18-21]. For the distributed formation control of USVs, the current main research direction is the non-time-varying formation control guided by multiple leaders, the shortcoming of which is that, according to the given communication topology, the formation can only be fixed but cannot change in response to the demand. In other words, when the demand changes, only by changing the topology can the desired performance be achieved, which lacks flexibility. Compared with non-time-varying formation control, distributed time-varying formation control method guided by multiple leaders can not only keep multiple USVs in fixed formation but also generate time-varying formation, which makes the formation flexible, easy to operate, etc. If there is no mission, under the guidance of multiple leaders, the USVs can take a fixed formation. On the contrary, if the mission requirements change, the USVs can be changed to the desired formation without changing the topology.

This paper investigates the distributed time-varying formation control of a swarm of under-actuated USVs guided by multiple leaders in the presence of complex model uncertainties and unknown ocean disturbances. Firstly, at the kinematic level, distributed time-varying formation guidance law is designed on the basis of the containment method and path maneuvering principles, and the basic formation is designed through information transfer relationships between USVs and between USVs and leaders. The guidance law is based on the information of neighbors (position, surge speed, and heading) and given a time-varying input signal to calculate the desired heading and surge speed of the following ships. Then, at the kinetic level, the surge speed and yaw rate control laws of USVs are developed on the basis of the extended state observer (ESO) method such that the influences of the model uncertainties and unknown ocean disturbances are mitigated. Further, cascade system stability analysis is undertaken to validate the input status stability of the closed-loop control system for the time-varying formation of USVs, and the effectiveness of the controller is demonstrated via simulation.

1 Problem description

This paper uses a time-varying formation system consisting of M twin-propeller USVs and $N-M$ virtual leaders, as shown in Fig. 1, where $\boldsymbol{p}_i=(x_i, y_i)$, representing the position of the i-th USV ($i \in M$) in the north-east-down (NED) reference frame X_E-Y_E; φ_i is the heading angle of the i-th USV in NED reference frame; θ_k is the parameter variable of the k-th ($k \in [M+1, N]$) parameterized path.

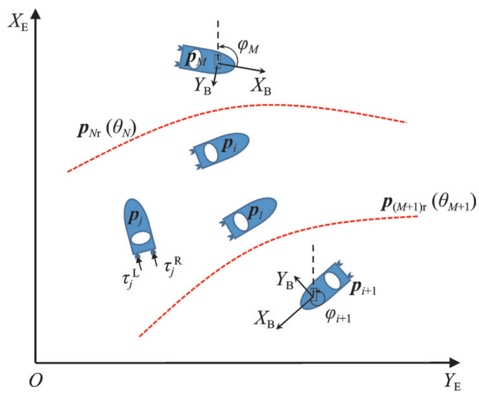

Fig.1 System structure of time-varying formation

At the kinematic level, the i-th USV can be represented by the state equation shown in Eq. (1) [22].

$$\begin{cases} \dot{x}_i = u_i \cos\varphi_i - v_i \sin\varphi_i \\ \dot{y}_i = u_i \sin\varphi_i + v_i \cos\varphi_i \\ \dot{\varphi}_i = r_i \end{cases} \tag{1}$$

where u_i, v_i and r_i are respectively the surge speed, side velocity, and yaw rate of the i-th USV in the body-fixed reference frame X_B-Y_B.

Based on the hydrodynamic equations of the USV at the surface, the kinetic equations of the USV can be obtained as shown in Eq. (2) [23].

downloaded from www.ship-research.com

$$\begin{cases} m_i^u \dot{u}_i = f_i^u(u_i, v_i, r_i) + \tau_i^u + \tau_{id}^u(t) \\ m_i^v \dot{v}_i = f_i^v(u_i, v_i, r_i) + \tau_{id}^v(t) \\ m_i^r \dot{r}_i = f_i^r(u_i, v_i, r_i) + \tau_i^r + \tau_{id}^r(t) \end{cases} \tag{2}$$

where m_i^u, m_i^v and m_i^r are the inertial coefficients of the i-th USV; $f_i^u(\cdot)$, $f_i^v(\cdot)$ and $f_i^r(\cdot)$ are disturbances caused by the model uncertainties of the i-th USV; $\tau_{id}^u(t)$, $\tau_{id}^v(t)$ and $\tau_{id}^r(t)$ are respectively the time-varying external disturbances of the i-th USV in the directions of surge speed u, side velocity v and yaw rate r; τ_i^u and τ_i^r are respectively the surge force and yaw control input of the i-th USV.

The under-actuated USV studied in this paper is propelled by twin propellers, and steering is provided through the speed differences of the propellers at different control inputs. Due to the control coupling of the surge speed and yaw rate of the USV, which is fixed by twin propellers, to simplify the design of the controller, we need to decouple the control inputs of these two parameters, namely that the control inputs of left and right propellers of the USV, τ_i^{L} and τ_i^{R}, are split [24] as shown in Eq. (3).

$$\begin{cases} \tau_i^{\mathrm{L}} = (1-\epsilon)\left(\tau_i^u/2 + \tau_i^r/d\right) \\ \tau_i^{\mathrm{R}} = (1-\epsilon)\left(\tau_i^u/2 - \tau_i^r/d\right) \end{cases} \tag{3}$$

where ϵ is the thrust deduction factor; d is the distance between two propellers.

In this paper, in order to perform the guiding function of the virtual leaders, we need to make them move along the known parameterized path, so the position of the parameterized path at moment t is the position of the virtual leaders. The parameterized path of the k-th virtual leader is set as $\boldsymbol{p}_{kr}(\theta_k(t)) = \mathrm{col}(x_k(\theta_k), y_k(\theta_k))$, $k=M+1, \ldots, N$, where θ_k, $x_k(\theta_k)$ and $y_k(\theta_k)$ are the parameters of the k-th leader path. To perform the synergistic movement of the USV and the virtual leaders, we design the derivative of the path parameters of the k-th virtual leader as follows:

$$\dot{\theta}_k = u_0 - \eta_k \tag{4}$$

where u_0 is the desired update rate for path parameters; η_k is the synergistic parameter for the USV and virtual leaders.

To perform the distributed time-varying formation control for USVs guided by multiple leaders, we make the following hypotheses:

Hypothesis 1: Each USV has at least one directed path from the virtual leaders to the USV and is able to obtain a time-varying input signal. Besides, the virtual leaders can communicate with each other.

Hypothesis 2: The parameterized path $\boldsymbol{p}_{kr}(\theta_k(t))$ and its first-order partial derivative $\dot{\boldsymbol{p}}_{kr}(\theta_k(t))$ are bounded.

In order to achieve the desired control effect of the movement of the USV, we should make the following control objectives satisfied:

1) Geometric targets: Each USV converges to a point within the convex combination of the virtual leader by a time-varying positional deviation $\boldsymbol{p}_{id}(t)$ according to Eq. (5), thus forming the desired distributed time-varying formation.

$$\lim_{t\to\infty} \left\| \boldsymbol{p}_i(t) - \sum_{k=M+1}^{N} \lambda_k \boldsymbol{p}_{kr}(\theta_k(t)) - \boldsymbol{p}_{id}(t) \right\| \leqslant \delta_1 \tag{5}$$

where $\boldsymbol{p}_i(t)$ is the position of the i-th USV in the NED reference frame at the moment of t; $\lambda_k \geqslant 0$ is the weight coefficient for the i-th USV and the k-th leader, and it meets $\sum_{k=M+1}^{N} \lambda_k = 1$; δ_1 is a positive number greater than zero; the given time-varying deviation signal $\boldsymbol{p}_{id}(t) = \mathrm{col}(x_{id}(t), y_{id}(t))$, $i = 1, \ldots, M$ is the time-varying positional deviation of the point within the convex combination of the virtual leader and the i-th USV, where $x_{id}(t)$ and $y_{id}(t)$ are respectively the components along the X_{E} and Y_{E} directions in the NED reference frame.

2) Dynamic targets: Each virtual leader moves at a given parameter update rate u_0 as shown in Eq. (6) to perform the desired formation structure.

$$\begin{cases} \lim_{t\to\infty} |\theta_k(t) - \theta_l(t)| \leqslant \delta_2 \\ \lim_{t\to\infty} |\dot{\theta}_k(t) - u_0| \leqslant \delta_3 \end{cases} \tag{6}$$

where k, $l = M+1, \ldots, N$, and $k \neq l$; $\theta_l(t)$ is the path parameter of the l-th virtual leader; δ_2 and $\delta_3 \in \mathbf{R}^+$ respectively, are some positive numbers greater than zero.

2 Controller design

This section mainly introduces the design of the UAV time-varying formation controller from the kinetics and kinematics aspects. The cascade system structure that makes up the controller is shown in Fig. 2.

2.1 Kinematic controller

According to containment method and the path maneuvering principles, the operation error e_i of the i-th USV in NED reference frame is defined as follows:

$$\boldsymbol{e}_i = \mathrm{col}(e_{ix}, e_{iy}) = \sum_{j=1}^{M} a_{ij}\left(\boldsymbol{p}_i - \boldsymbol{p}_{ijd} - \boldsymbol{p}_j\right) + \sum_{k=M+1}^{N} a_{ik}(\boldsymbol{p}_i - \boldsymbol{p}_{id} - \boldsymbol{p}_{kr}) \tag{7}$$

where e_{ix} and e_{iy} are the errors along the directions of

downloaded from www.ship-research.com

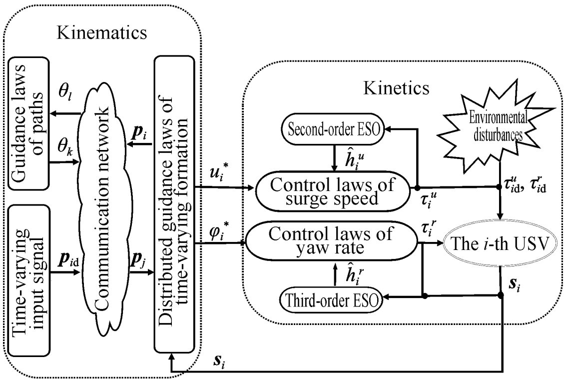

Fig. 2 System structure of time-varying formation

X_{E} and Y_{E} in NED reference frame, respectively; when the i-th USV can obtain the information from the j-th USV, $a_{ij}=1$, otherwise $a_{ij}=0$; when the information from the k-th virtual leader can be obtained, $a_{ik}=1$, otherwise $a_{ik}=0$; $\boldsymbol{p}_{ij\mathrm{d}}=\boldsymbol{p}_{i\mathrm{d}}-\boldsymbol{p}_{j\mathrm{d}}$ is the given time-varying positional deviation signal between the i-th USV and the j-th USV.

According to the kinematic state equations for USV in Eq. (1) and parameter update laws for virtual leaders in Eq. (4), there is the partial derivative of operation error $\boldsymbol{e}_i$:

$$\dot{\boldsymbol{e}}_i = c_i\left[u_i\boldsymbol{g}_u(\varphi_i)+v_i\boldsymbol{g}_v(\varphi_i)\right]-\sum_{j=1}^{M}a_{ij}\left[\left(u_j\boldsymbol{g}_u(\varphi_j)+v_j\boldsymbol{g}_v(\varphi_j)\right)+\dot{\boldsymbol{p}}_{ij\mathrm{d}}\right]-\sum_{k=M+1}^{N}a_{ik}\left[\dot{\boldsymbol{p}}_{k\mathrm{r}}(u_0-\eta_k)+\dot{\boldsymbol{p}}_{i\mathrm{d}}\right] \tag{8}$$

where $\boldsymbol{g}_u(\varphi_i)=\mathrm{col}(\cos(\varphi_i),\ \sin(\varphi_i))$, $\boldsymbol{g}_v(\varphi_i)=\mathrm{col}(-\sin(\varphi_i),\cos(\varphi_i))$, $i=1,\dots,M$, $c_i=\sum_{j=1}^{N}a_{ij}$.

In order to stabilize the operation error $\boldsymbol{e}_i$ in Eq. (8), we design the distributed guidance laws for time-varying formation shown in Eq. (9).

$$\boldsymbol{\alpha}_i=\mathrm{col}\left(\alpha_{ix},\alpha_{iy}\right)=\mathrm{col}\left(u_i^*\cos\varphi_i^*,u_i^*\sin\varphi_i^*\right)=\frac{1}{c_i}\left\{-\frac{\boldsymbol{K}_{\mathrm{c}i}\boldsymbol{e}_i}{\sqrt{\|\boldsymbol{e}_i\|^2+\delta_{i1}^2}}+\sum_{j=1}^{M}a_{ij}\left(u_j\boldsymbol{g}_u\left(\varphi_j\right)+v_j\boldsymbol{g}_v\left(\varphi_j\right)+\dot{\boldsymbol{p}}_{ij\mathrm{d}}\right)+\sum_{k=M+1}^{N}a_{ik}\left(u_0\dot{\boldsymbol{p}}_{k\mathrm{r}}+\dot{\boldsymbol{p}}_{i\mathrm{d}}\right)\right\}-v_j\boldsymbol{g}_v\left(\varphi_j\right) \tag{9}$$

where u_i^* and φ_i^* are respectively the desired heading and surge speed of the i-th USV; $\boldsymbol{K}_{\mathrm{c}i}=\mathrm{diag}\{k_{\mathrm{c}i1},k_{\mathrm{c}i2}\}\in\mathbf{R}^{2\times2}$ is the kinematic gain matrix; $\delta_{i1}\in\mathbf{R}$ is the parameter preventing the saturation of the surge speed.

According to Eq. (9), the desired surge speed and heading angle of the i-th USV are respectively as follows:

$$\begin{cases} u_i^*=\|\boldsymbol{\alpha}_i\|\cos\left(\varphi_i-\varphi_i^*\right)\\ \varphi_i^*=\mathrm{atan2}\left(\alpha_{iy},\alpha_{ix}\right),\ i=1,\dots,M \end{cases} \tag{10}$$

In order to perform the synergistic movement on USVs and virtual leaders, we design the synergistic parameter η_k as

$$\eta_k=-\varsigma_k\sigma_k=-\varsigma_k(\sigma_{k1}-\sigma_{k2}) \tag{11}$$

where ς_k is the synergistic gain constant; σ_k is the synergistic error divided into two parts: $\sigma_{k1}=\sum_{k=M+1}^{N}a_{ik}\dot{\boldsymbol{p}}_{k\mathrm{r}}^{\mathrm{T}}\boldsymbol{e}_i$ representing the path update rate calculated from the information of USVs by virtual leaders, and $\sigma_{k2}=\sum_{l=M+1}^{N}a_{kl}(\theta_k-\theta_l)+a_{k0}(\theta_k-\theta_0)$, representing that when the k-th virtual leader is able to obtain the path information of the super leader, $a_{k0}=1$, otherwise $ak_0=0$; θ_0 is the path update parameter of the super leader, and $\dot{\theta}_0=u_0$.

The synergistic error of the global path variable is defined as $\theta_{k\mathrm{e}}=\theta_k-\theta_0$, and it meets

$$\dot{\theta}_{k\mathrm{e}}=-\eta_k \tag{12}$$

The synergistic error vector of global path variable is set as $\boldsymbol{\theta}_{\mathrm{e}}=\mathrm{col}(\theta_{(M+1)\mathrm{e}},\dots,\theta_{N\mathrm{e}})$, and the synergistic error vector of partial path variable is set as $\boldsymbol{z}=\mathrm{col}(z_{M+1},\dots,z_N)$, which meets $\boldsymbol{z}=\boldsymbol{C}\boldsymbol{\theta}_{\mathrm{e}}$ $\boldsymbol{C}=\boldsymbol{A}_0+\boldsymbol{B}_0$. Here, $\boldsymbol{A}_0=\left[a_{ij}\right]\in\mathbf{R}^{(N-M)(N-M)}$ and it is the communication matrix for virtual leaders. When the i-th leader can obtain the information from the j-th leader, $a_{ij}=1$, otherwise $a_{ij}=0$; $\boldsymbol{B}_0=\mathrm{diag}\{a_{(M+1)0},\dots,a_{N0}\}$ is the matrix of leaders.

Substituting Eq. (9) into Eqs. (8) and (12), we can obtain the dynamic error of kinematic system represented respectively as follows:

$$\begin{cases} \dot{\boldsymbol{e}}_i=-\dfrac{\boldsymbol{K}_{\mathrm{c}i}\boldsymbol{e}_i}{\sqrt{\|\boldsymbol{e}_i\|^2+\delta_{i1}^2}}+c_i\boldsymbol{\varDelta}_{i\mathrm{e}}+\sum\limits_{k=M+1}^{N}a_{ik}\eta_k\dot{\boldsymbol{p}}_{k\mathrm{r}}\\ \dot{\theta}_{k\mathrm{e}}=-\eta_k \end{cases} \tag{13}$$

where $\boldsymbol{\varDelta}_{i\mathrm{e}}=u_i\boldsymbol{g}_u(\varphi_i)-u_i^*\boldsymbol{g}_u\left(\varphi_i^*\right)$ is the kinetic tracking error vector.

2.2 Kinetic controller

In Section 2.1, based on containment method and path maneuvering principles, this paper designs desired headings and surge speed for multiple USVs. In this section, this paper uses ESO to estimate model uncertainties and unknown ocean disturbances. Then, on this basis, kinetic control laws of ESO are designed to make the actual speed and headings of USVs meet the requirements of desired values.

Because the adopted USV uses an under-actuated unmanned system, in order to simplify the design of

downloaded from www.ship-research.com

ESO, we rewrite Eq. (2) as follows:

$$\begin{cases} \dot{u}_i = \tau_i^u / m_i^u + h_i^u(u_i, r_i, t) \\ \dot{r}_i = \tau_i^r / m_i^r + h_i^r(u_i, r_i, t) \end{cases} \tag{14}$$

where $h_i^u(u_i, r_i, t) = \left(f_i^u(u_i, v_i, r_i) + \tau_{id}^u(t)\right)/m_i^u$, $h_i^r(u_i, r_i, t) = \left(f_i^r(u_i, v_i, r_i) + \tau_{id}^r(t)\right)/m_i^r$ are both unknown functions.

The design and analysis of ESO are assumed as follows:

Hypothesis 3: The derivatives of h_i^u and h_i^r (disturbances caused by model uncertainties and unknown environmental disturbances) are bounded and meet $\left|\dot{h}_i^u\right| + \left|\dot{h}_i^r\right| \leqslant h_i^*$, where h_i^* is an arbitrary positive number.

1) The design of control laws for the surge speed: Because there are uncertainties and unknown ocean disturbances in USV model, the following second-order ESO system is designed for estimating the unknown h_i^u.

$$\begin{cases} \dot{\hat{u}}_i = -\mu_{i1}^u \tilde{u}_i + \hat{h}_i^u + \tau_i^u / m_i^u \\ \dot{\hat{h}}_i^u = -\mu_{i2}^u \tilde{u}_i \end{cases} \tag{15}$$

where $\mu_{i1}^u, \mu_{i2}^u \in \mathbf{R}^+$ and they are ESO observer gain; $\hat{u}_i$, $\hat{h}_i^u$ are respectively the estimated values of u_i and h_i^u; $\tilde{u}_i = \hat{u}_i - u_i$, is the estimated error of the surge speed. The estimated error of h_i^u is defined as $\tilde{h}_i^u = \hat{h}_i^u - h_i^u$. Combining Eqs. (14) and (15), we can obtain the dynamic error expression of second-order ESO as follows:

$$\begin{cases} \dot{\tilde{u}}_i = -\mu_{i1}^u \tilde{u}_i + \tilde{h}_i^u \\ \dot{\tilde{h}}_i^u = -\mu_{i2}^u \tilde{u}_i - \dot{h}_i^u \end{cases} \tag{16}$$

The tracking error of desired surge speed is set as $\hat{u}_i^* = \hat{u}_i - u_i^*$. Its derivative with respect to is as follows:

$$\dot{\hat{u}}_i^* = -\mu_{i1}^u \tilde{u}_i + \hat{h}_i^u + \tau_i^u / m_i^u - \dot{u}_i^* \tag{17}$$

According to Eq. (15), active-disturbance-rejection control laws of surge speed shown in Eq. (18) is designed to stabilize $\dot{\hat{u}}_i^*$:

$$\tau_i^u = -\frac{\mu_{ic}^u \hat{u}_i^*}{\sqrt{\left|\hat{u}_i^*\right|^2 + \delta_{i2}^2}} - \hat{h}_i^u + \dot{\mu}_i^* \tag{18}$$

where $\mu_{ic}^u \in \mathbf{R}^+$ is a kinetic gain constant; $\delta_{i2} \in \mathbf{R}$ is a positive number. Coupling Eqs. (17) and (18) yields the dynamic form of $\dot{\hat{u}}_i^*$:

$$\dot{\hat{u}}_i^* = -\frac{\mu_{ic}^u \hat{u}_i^*}{\sqrt{\left|\hat{u}_i^*\right|^2 + \delta_{i2}^2}} - \mu_{i1}^u \tilde{u}_i \tag{19}$$

Eq. (16) is rewritten into a matrix as follows:

$$\dot{\boldsymbol{E}}_{i1} = \boldsymbol{B}_{i1} \boldsymbol{E}_{i1} + \boldsymbol{C}_{i1} \dot{h}_i^u \tag{20}$$

where $\boldsymbol{E}_{i1} = \mathrm{col}\left(\tilde{u}_i, \tilde{h}_i^u\right)$, $\boldsymbol{B}_{i1} = \left[\, -\mu_{i1}^u \;\; 1 \;;\; -\mu_{i2}^u \;\; 0 \,\right]$, $\boldsymbol{C}_{i1}$=col(0, −1). Because $\boldsymbol{B}_{i1}$ is a Hurwitz matrix, there is a positive definite matrix $\boldsymbol{P}_{i1}$, which makes $\boldsymbol{B}_{i1}$ meet the following inequality:

$$\boldsymbol{B}_{i1}^{\mathrm{T}} \boldsymbol{P}_{i1} + \boldsymbol{P}_{i1} \boldsymbol{B}_{i1} \leqslant -\xi_{i1} \boldsymbol{I}_2 \tag{21}$$

where ξ_{i1} is a positive number; $\boldsymbol{I}_2$ is a two-dimensional identity matrix.

2) The design of control laws for the yaw rate: Similar to the design of control laws for the surge speed, this paper uses third-order ESO for estimating the unknown h_i^r, and the following expression for third-order ESO system is designed:

$$\begin{cases} \dot{\hat{\varphi}}_i = -\mu_{i1}^\varphi \tilde{\varphi}_i + \hat{r}_i \\ \dot{\hat{r}}_i = -\mu_{i2}^\varphi \tilde{\varphi}_i + \hat{h}_i^r + \tau_i^r / m_i^r \\ \dot{\hat{h}}_i^r = -\mu_{i3}^\varphi \tilde{\varphi}_i \end{cases} \tag{22}$$

where $\mu_{i1}^\varphi, \mu_{i2}^\varphi, \mu_{i3}^\varphi \in \mathbf{R}^+$ are all ESO observer gain; $\hat{\varphi}_i$, $\hat{r}_i$ and $\hat{h}_i^r$ are respectively the estimated values of φ_i, r_i and h_i^r; $\tilde{\varphi}_i = \hat{\varphi}_i - \varphi_i$, is the estimated error of heading angle. The estimated errors of r_i and h_i^r are respectively $\tilde{r}_i = \hat{r}_i - r_i$, $\tilde{h}_i^r = \hat{h}_i^r - h_i^r$. Coupling Eqs. (14) and (22), we can obtain the dynamic error expression for third-order ESO as follows:

$$\begin{cases} \dot{\tilde{\varphi}}_i = -\mu_{i1}^\varphi \tilde{\varphi}_i + \tilde{r}_i \\ \dot{\tilde{r}}_i = -\mu_{i2}^\varphi \tilde{\varphi}_i + \tilde{h}_i^r \\ \dot{\tilde{h}}_i^r = -\mu_{i3}^\varphi \tilde{\varphi}_i - \dot{h}_i^r \end{cases} \tag{23}$$

It is assumed that $\hat{\varphi}_i^*$ and $\hat{r}_i^*$ are respectively the estimated tracking errors of the desired heading angle and desired yaw rate, i.e., $\hat{\varphi}_i^* = \hat{\varphi}_i - \varphi_i^*$, $\hat{r}_i^* = \hat{r}_i - r_i^*$. Coupling Eq. (22) and taking the derivative of $\hat{\varphi}_i^*$ and $\hat{r}_i^*$, we have

$$\begin{cases} \dot{\hat{\varphi}}_i^* = -\mu_{i1}^\varphi \tilde{\varphi}_i + \hat{r}_i - \dot{\varphi}_i^* \\ \dot{\hat{r}}_i^* = -\mu_{i2}^\varphi \tilde{\varphi}_i + \hat{h}_i^r + \tau_i^r / m_i^r - \dot{r}_i^* \end{cases} \tag{24}$$

The desired virtual angular speed shown in Eq. (25) is designed to stabilize $\dot{\hat{\varphi}}_i^*$.

$$r_i^* = -\frac{\mu_{ic}^\varphi \hat{\varphi}_i^*}{\sqrt{\hat{\varphi}_i'^2 + \delta_{i3}^2}} + \hat{\varphi}_i^* \tag{25}$$

where $\mu_{ic}^\varphi \in \mathbf{R}$ is kinetic gain constant; δ_{i3} is a positive number. Based on Eq. (22), this paper designs control laws for the yaw rate shown in Eq. (26) to stabilize $\dot{\hat{r}}_i^*$.

$$\tau_i^r = m_i^r \left(-\frac{\mu_{ic}^r \hat{r}_i^*}{\sqrt{\left|\hat{r}_i^*\right|^2 + \delta_{i4}^2}} - \hat{h}_i^r + \dot{r}_i^* - \hat{\varphi}_i^* \right) \tag{26}$$

where $\mu_{ic}^r \in \mathbf{R}$ is kinetic gain constant; δ_{i4} is a positive number. Coupling Eqs. (24)–(26), we can rewrite the derivative of $\hat{\varphi}_i^*$ and $\hat{r}_i^*$ as follows:

downloaded from www.ship-research.com

$$\begin{cases} \dot{\hat{\varphi}}_i^* = -\dfrac{\mu_{ic}^{\varphi}\hat{\varphi}_i^*}{\sqrt{\hat{\varphi}_i'^2+\delta_{i3}^2}} - \mu_{i1}^{\varphi}\tilde{\varphi}_i + \hat{r}_i^* \\ \dot{\hat{r}}_i^* = -\dfrac{\mu_{ic}^{r}\hat{r}_i^*}{\sqrt{\left|\hat{r}_i^*\right|^2+\delta_{i4}^2}} - \mu_{i2}^{\varphi}\tilde{\varphi}_i - \hat{\varphi}_i^* \end{cases} \tag{27}$$

Eq. (23) is adapted into a matrix as follows:

$$\dot{\boldsymbol{E}}_{i2} = \boldsymbol{B}_{i2}\boldsymbol{E}_{i2} + \boldsymbol{C}_{i2}\dot{h}_i^r \tag{28}$$

where

$$\boldsymbol{E}_{i2} = \mathrm{col}\left(\tilde{\varphi}_i, \tilde{r}_i, \tilde{h}_i^r\right), \ \boldsymbol{C}_{i2} = \mathrm{col}(0,0,-1)$$

$$\boldsymbol{B}_{i2} = \begin{bmatrix} -\mu_{i1}^{\varphi} & 1 & 0 \\ -\mu_{i2}^{\varphi} & 0 & 1 \\ -\mu_{i3}^{\varphi} & 0 & 0 \end{bmatrix}$$

Because $\boldsymbol{B}_{i2}$ is a Hurwitz matrix, there should be a positive definite matrix $\boldsymbol{P}_{i2}$ making $\boldsymbol{B}_{i2}$ meet the following inequality:

$$\boldsymbol{B}_{i2}^{\mathrm{T}}\boldsymbol{P}_{i2} + \boldsymbol{P}_{i2}\boldsymbol{B}_{i2} \leqslant -\xi_{i2}\boldsymbol{I}_3 \tag{29}$$

where ξ_{i2} is a positive number; $\boldsymbol{I}_3$ is a three-dimensional identity matrix.

3 Stability analysis

3.1 Demonstration of the stability of ESO subsystem

This section will demonstrate the stability of ESO subsystem proposed in Section 2.2. Considering that the subsystems in Eqs. (20) and (28) are in the same form, this section mainly introduces the demonstration of the stability of ESO subsystem shown in Eq. (20), which is given by Lemma 1.

Lemma 1: Under Hypothesis 3, the ESO subsystem shown in Eq. (20): $\left[\dot{h}_i^u\right] \mapsto [\boldsymbol{E}_{i1}]$ is input-to-state stable (ISS).

Proof: Lyapunov equation is built as follows:

$$V_1 = \frac{1}{2}\sum_{i=1}^{M}\boldsymbol{E}_{i1}^{\mathrm{T}}\boldsymbol{P}_{i1}\boldsymbol{E}_{i1} \tag{30}$$

Taking the derivative of V_1, we have

$$\dot{V}_1 = \sum_{i=1}^{M}\boldsymbol{E}_{i1}^{\mathrm{T}}\boldsymbol{P}_{i1}\left(\boldsymbol{B}_{i1}\boldsymbol{E}_{i1} + \boldsymbol{C}_{i1}\dot{h}_i^u\right) \tag{31}$$

Coupling Eq. (21) and Eq. (31), we have

$$\dot{V}_1 \leqslant \sum_{i=1}^{M}\left(-\frac{\xi_{i1}}{2}\|\boldsymbol{E}_{i1}\|^2 + \|\boldsymbol{E}_{i1}\|\|\boldsymbol{P}_{i1}\boldsymbol{C}_{i1}\|\left|\dot{h}_i^u\right|\right) \tag{32}$$

When it meets $\|\boldsymbol{E}_{i1}\| \geqslant 2\|\boldsymbol{P}_{i1}\boldsymbol{C}_{i1}\|\left|\dot{h}_i^u\right|/(\xi_{i1}\varepsilon_{i1})$, there is

$$\dot{V}_1 \leqslant -\sum_{i=1}^{M}\frac{\xi_{i1}}{2}(1-\varepsilon_{i1})\|\boldsymbol{E}_{i1}\|^2 \tag{33}$$

where $0<\varepsilon_{i1}<1$. According to Theorem 4.6 in Reference [25], it can be seen that the ESO subsystem is ISS, and the boundary of $\|\boldsymbol{E}_{i1}\|$ can be represented as

$$\|\boldsymbol{E}_{i1}\| \leqslant \max\left\{\|\boldsymbol{E}_{i1}(t_0)\|\mathrm{e}^{-\xi_{i1}(1-\varepsilon_{i1})(t-t_0)/2}, \frac{2\|\boldsymbol{P}_{i1}\boldsymbol{C}_{i1}\|\sqrt{\lambda_{\max}(\boldsymbol{P}_{i1})}}{\xi_{i1}\varepsilon_{i1}\sqrt{\lambda_{\min}(\boldsymbol{P}_{i1})}}\left|\dot{h}_i^u\right|\right\}, \ \forall t \geqslant t_0 \tag{34}$$

Lemma 2: According to Hypothesis 3, the ESO subsystem shown in Eq. (28), $\left[\dot{h}_i^r\right] \mapsto [\boldsymbol{E}_{i2}]$, is ISS, and the boundary of $\|\boldsymbol{E}_{i2}\|$ can be represented as

$$\|\boldsymbol{E}_{i2}\| \leqslant \max\left\{\|\boldsymbol{E}_{i2}(t_0)\|\mathrm{e}^{-\xi_{i2}(1-\varepsilon_{i2})(t-t_0)/2}, \frac{2\|\boldsymbol{P}_{i2}\boldsymbol{C}_{i2}\|\sqrt{\lambda_{\max}(\boldsymbol{P}_{i2})}}{\xi_{i2}\varepsilon_{i2}\sqrt{\lambda_{\min}(\boldsymbol{P}_{i2})}}\left|\dot{h}_i^r\right|\right\}, \ \forall t \geqslant t_0 \tag{35}$$

where $0 < \varepsilon_{i2} < 1$; $\lambda_{\min}(\cdot)$ and $\lambda_{\max}(\cdot)$ are respectively the minimum and maximum eigenvalues of the matrix; t_0 is the initial time.

3.2 Demonstration of the stability of kinetic system

The kinetic system stability composed of Eq. (19) and Eq. (27) is given by Lemma 3.

Lemma 3: The kinetic system shown in Eq. (19) and Eq. (27), $[\tilde{u}_i, \tilde{\varphi}_i] \mapsto \left[\hat{u}_i^*, \hat{\varphi}_i^*, \hat{r}_i^*\right]$ is ISS.

Proof: Lyapunov equation is built as follows:

$$V_2 = \frac{1}{2}\sum_{i=1}^{M}\left(\hat{u}_i^{*2} + \hat{\varphi}_i^{*2} + \hat{r}_i^{*2}\right) \tag{36}$$

Combining Eq. (19), Eq. (27) and Eq. (36), and taking the derivative of V_2, we have

$$\dot{V}_2 = \sum_{i=1}^{M}\left(-\frac{\mu_{ic}^u}{\sqrt{\left|\hat{u}_i^*\right|^2+\delta_{i2}^2}} - \mu_{i1}^u\hat{u}_i\hat{u}_i^* - \frac{\mu_{ic}^{\varphi}}{\sqrt{\left|\hat{\varphi}_i^*\right|^2+\delta_{i3}^2}} - \mu_{i1}^{\varphi}\tilde{\varphi}_i\hat{\varphi}_i^* - \frac{\mu_{ic}^r}{\sqrt{\left|\hat{r}_i^*\right|^2+\delta_{i4}^2}} - \mu_{i1}^{\varphi}\tilde{\varphi}_i\hat{r}_i^*\right) \tag{37}$$

Let

$$\boldsymbol{\Gamma}_{ic} = \mathrm{diag}\left\{\mu_{ic}^u/\sqrt{\left|\hat{u}_i^*\right|^2+\delta_{i2}^2}, \mu_{ic}^{\varphi}/\sqrt{\left|\hat{\varphi}_i^*\right|^2+\delta_{i3}^2}, \mu_{ic}^r/\sqrt{\left|\hat{r}_i^*\right|^2+\delta_{i4}^2}\right\}$$

$$\boldsymbol{E}_{i3} = \mathrm{col}(\hat{u}_i^*, \hat{\varphi}_i^*, r_i^*)$$

The following inequality comes into existence:

$$\dot{V}_2 \leqslant -\sum_{i=1}^{M}\lambda_{\min}(\boldsymbol{\Gamma}_{ic})(1-\varepsilon_{i3})\|\boldsymbol{E}_{i3}\|^2 \tag{38}$$

where $0 < \varepsilon_{i3} < 1$.

According to Lemma 1 and Lemma 2, the kinetic system composed of Eq. (19) and Eq. (27) is ISS, and the boundary of $\|\boldsymbol{E}_{i3}\|$ can be represented as

downloaded from www.ship-research.com

$$\|\boldsymbol{E}_{i3}(t)\| \leqslant \max\left\{\|\boldsymbol{E}_{i3}(t_0)\| \mathrm{e}^{-\lambda_{\min}(\boldsymbol{\Gamma}_{ic})(1-\varepsilon_{i3})(t-t_0)}, \frac{\mu_{i1}^u\|\boldsymbol{E}_{i1}\|+\left(\mu_{i1}^\varphi+\mu_{i2}^\varphi\right)\|\boldsymbol{E}_{i2}\|}{\varepsilon_{i3}\lambda_{\min}(\boldsymbol{\Gamma}_{ic})}\right\}, \ \forall t \geqslant t_0 \tag{39}$$

With consideration of the tracking error of kinetic surge speed $u_{ie}=u_i-u_i^*=\hat{u}_i^*-\tilde{u}_i \leqslant \left|\hat{u}_i^*\right|-|\tilde{u}_i|$ and the tracking error of yaw rate $\varphi_{ie}=\varphi_i-\varphi_i^*=\hat{\varphi}_i^*-\tilde{\varphi}_i \leqslant \left|\hat{\varphi}_i^*\right|-|\tilde{\varphi}_i|$, kinetic tracking error is bounded, as can be seen from Eq. (34), Eq. (35) and Eq. (39).

3.3 Demonstration of the stability of kinematic system

The kinematic subsystem stability shown in Eq. (13) is given by Lemma 4.

Lemma 4: In Eq. (13) of kinematic subsystem, $[\boldsymbol{\varDelta}_{ie}] \mapsto [\boldsymbol{e}_i, \theta_{ie}]$ is ISS.

Proof: Lyapunov equation is built as follows:

$$V_3=\frac{1}{2}\sum_{i=1}^{M}\boldsymbol{e}_i^{\mathrm{T}}\boldsymbol{e}_i+\frac{1}{2}\boldsymbol{\theta}_{\mathrm{e}}^{\mathrm{T}}\boldsymbol{C}\boldsymbol{\theta}_{\mathrm{e}} \tag{40}$$

Coupling Eq. (13) and taking the derivative of V_3, we have

$$\dot{V}_3=\sum_{i=1}^{M}\left(-\boldsymbol{e}_i^{\mathrm{T}}K_{\mathrm{c}i}\boldsymbol{e}_i/\sqrt{\|\boldsymbol{e}_i\|^2+\delta_{i1}^2}+c_i\boldsymbol{e}_i^{\mathrm{T}}\boldsymbol{\varDelta}_{ie}\right)-\sum_{k=M+1}^{N}\varsigma_k\sigma_k^2 \tag{41}$$

It is assumed that $\boldsymbol{E}_1=\mathrm{col}(\boldsymbol{e}^{\mathrm{T}},\boldsymbol{\sigma}^{\mathrm{T}})$, $\boldsymbol{E}_2=\mathrm{col}(\boldsymbol{e}^{\mathrm{T}},\boldsymbol{\theta}_{\mathrm{e}}^{\mathrm{T}})$, which meet $\boldsymbol{E}_1=\boldsymbol{\Psi}\boldsymbol{E}_2$, $\boldsymbol{e}=\mathrm{col}\left(\boldsymbol{e}_1^{\mathrm{T}},\ldots,\boldsymbol{e}_k^{\mathrm{T}}\right)$, $\boldsymbol{\sigma}=\mathrm{col}(\sigma_{M+1},\cdots\ \sigma_N)$.

Where

$$\boldsymbol{\Psi}=\begin{bmatrix}\boldsymbol{I}_M\otimes\boldsymbol{I}_2 & \boldsymbol{0}\\ \boldsymbol{\Upsilon}^{\mathrm{T}} & -\boldsymbol{C}\end{bmatrix}$$

$$\boldsymbol{\Upsilon}=\begin{bmatrix}a_{(M+1)1}\dot{\boldsymbol{p}}_{(M+1)\mathrm{r}} & \cdots & a_{N1}\dot{\boldsymbol{p}}_{N\mathrm{r}}\\ \vdots & \ddots & \vdots\\ a_{(M+1)M}\dot{\boldsymbol{p}}_{(M+1)\mathrm{r}} & \cdots & a_{NM}\dot{\boldsymbol{p}}_{N\mathrm{r}}\end{bmatrix}$$

Thus, there is an inequality:

$$\dot{V}_3 \leqslant -\lambda\|\boldsymbol{E}_1\|^2+\|\boldsymbol{c}\|\|\boldsymbol{\varDelta}_{\mathrm{e}}\|\|\boldsymbol{E}_1\| \leqslant -\lambda\lambda_{\min}(\boldsymbol{\Psi})\|\boldsymbol{E}_2\|^2+\lambda_{\max}(\boldsymbol{\Psi})\|\boldsymbol{c}\|\|\boldsymbol{\varDelta}_{\mathrm{e}}\|\|\boldsymbol{E}_2\| \tag{42}$$

where

$$\boldsymbol{c}=\mathrm{diag}(c_1\otimes\boldsymbol{I}_2,\ldots,c_M\otimes\boldsymbol{I}_2)$$

$$\lambda=\left\{\lambda_{\min}\left(K_{\mathrm{c}i}\boldsymbol{e}_i/\sqrt{\|\boldsymbol{e}_i\|^2+\delta_{i1}^2}\right),\varsigma_k\right\}_{\min}$$

$$i=1,\ldots,M;\ k=M+1,\ldots,N$$

$$\boldsymbol{\varDelta}_{\mathrm{e}}=\mathrm{col}\left(\boldsymbol{\varDelta}_{1\mathrm{e}}^{\mathrm{T}},\ldots,\boldsymbol{\varDelta}_{M\mathrm{e}}^{\mathrm{T}}\right)$$

$\boldsymbol{E}_2$ meets the following relationship:

$$\|\boldsymbol{E}_2\| \geqslant \frac{\lambda_{\max}(\boldsymbol{\Psi})\|\boldsymbol{c}\|\|\boldsymbol{\varDelta}_{\mathrm{e}}\|}{\lambda\varepsilon_4\lambda_{\min}(\boldsymbol{\Psi})} \tag{43}$$

where $0<\varepsilon_4<1$.

Coupling Eq. (42) and Eq. (43), we have

$$\dot{V}_3 \leqslant -\lambda\lambda_{\min}(\boldsymbol{\Psi})(1-\varepsilon_4)\|\boldsymbol{E}_2\|^2 \tag{44}$$

It can be seen from Lemma 3 that, input signal Δ_{e} is bounded, and there is a positive number Δ_{e}^*, meeting $\|\Delta_{\mathrm{e}}\| \leqslant \Delta_{\mathrm{e}}^*$. Thus, the kinematic system shown in Eq. (13) is ISS, and the boundary of $\|\boldsymbol{E}_2\|$ can be represented as

$$\|\boldsymbol{E}_2(t)\| \leqslant \max\left\{\|\boldsymbol{E}_2(t_0)\|\mathrm{e}^{-\lambda\lambda_{\min}(\boldsymbol{\Psi})(1-\varepsilon_4)(t-t_0)}, \frac{\lambda_{\max}(\boldsymbol{\Psi})\|\boldsymbol{c}\|\|\boldsymbol{\varDelta}_{\mathrm{e}}\|}{\lambda\varepsilon_4\lambda_{\min}(\boldsymbol{\Psi})}\right\}, \ \forall t \geqslant t_0 \tag{45}$$

3.4 Demonstration of the stability of cascade system

For USVs with twin propellers and guided by multiple leaders, the stability of cascade system for their time-varying formation control system can be given through Theorem 1.

Theorem 1: Considering the distributed time-varying formation for USVs guided by multiple leaders, the kinestate of USVs can be expressed by the mathematical model shown in Eqs. (1) and (2). The controller consists of the kinematic guidance laws shown in Eq. (10), path update laws shown in Eq. (11), ESO predictor shown in Eq. (20) and Eq. (28), and kinetic control laws shown in Eq. (18) and Eq. (26). If it meets Hypotheses 1-3, the closed-loop control system of time-varying formation for USVs guided by multiple paths is ISS.

Proof: Based on Lemmas 1-4, the cascade system composed of subsystems shown in Eqs. (13), (19), (20), (27), and (28) is ISS. When $t\to\infty$, it meets the following relationships:

$$\begin{cases}\|\boldsymbol{E}_{i1}(t)\|_{t\to\infty} \leqslant \dfrac{2\|\boldsymbol{P}_{i1}\boldsymbol{C}_{i1}\|\sqrt{\lambda_{\max}(\boldsymbol{P}_{i1})}}{\xi_{i1}\varepsilon_{i1}\sqrt{\lambda_{\min}(\boldsymbol{P}_{i1})}}h_i^*\\ \|\boldsymbol{E}_{i2}(t)\|_{t\to\infty} \leqslant \dfrac{2\|\boldsymbol{P}_{i2}\boldsymbol{C}_{i2}\|\sqrt{\lambda_{\max}(\boldsymbol{P}_{i2})}}{\xi_{i2}\varepsilon_{i2}\sqrt{\lambda_{\min}(\boldsymbol{P}_{i2})}}h_i^*\\ \|\boldsymbol{E}_{i3}(t)\|_{t\to\infty} \leqslant \dfrac{2\mu_{i1}^u\delta_{i3}\|\boldsymbol{P}_{i1}\boldsymbol{C}_{i1}\|\sqrt{\lambda_{\max}(\boldsymbol{P}_{i1})}}{\xi_{i1}\varepsilon_{i1}\varepsilon_{i3}\sqrt{\lambda_{\min}(\boldsymbol{\Gamma}_{ic})}\sqrt{\lambda_{\min}(\boldsymbol{P}_{i1})}}+\\ \qquad \dfrac{2\delta_{i3}\left(\mu_{i1}^\varphi+\mu_{i2}^\varphi\right)\|\boldsymbol{P}_{i2}\boldsymbol{C}_{i2}\|\sqrt{\lambda_{\max}(\boldsymbol{P}_{i2})}}{\xi_{i2}\varepsilon_{i1}\varepsilon_{i3}\sqrt{\lambda_{\min}(\boldsymbol{\Gamma}_{ic})}\sqrt{\lambda_{\min}(\boldsymbol{P}_{i2})}}\\ \|\boldsymbol{E}_2(t)\|_{t\to\infty} \leqslant \dfrac{\boldsymbol{\varDelta}_{\mathrm{e}}^*\lambda_{\max}(\boldsymbol{\Psi})\|\boldsymbol{c}\|}{\lambda\varepsilon_4\lambda_{\min}(\boldsymbol{\Psi})}\end{cases} \tag{46}$$

4 Simulation results

This section verifies the distributed time-varying formation system for USVs guided by multiple leaders through simulation. By the system composed of six USVs and two virtual leaders, which is shown in Fig. 3, the effectiveness of discussed control laws is verified.

downloaded from www.ship-research.com

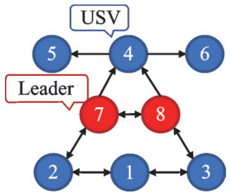

Fig.3 Communication network structure of time-varying formation system

As shown in Fig. 3, the lines between any two USVs indicate the information transfer between them, and the arrows indicate the direction of information flow. The corresponding communication structure of the simulation is as follows: 2#–4# USVs can get the path information of the virtual leader, and 1#, 5# and 6# USVs can only get the information of neighboring USVs.

The physical parameters of USV in this simulation come from Reference [26]. Parameters needed in this paper are elaborated as follows: The initial status information of the i-th USV is represented as $\boldsymbol{s}_i$= col(x_i, y_i, φ_i, u_i, v_i, r_i) and the initial status information of 1#–6# USVs is respectively represented as follows:

$$\boldsymbol{s}_1=\mathrm{col}(35,-90,\pi,0,0,0),\ \boldsymbol{s}_2=\mathrm{col}(35,-100,\pi,0,0,0)$$
$$\boldsymbol{s}_3=\mathrm{col}(35,-75,\pi,0,0,0),\ \boldsymbol{s}_4=\mathrm{col}(25,-70,\pi/2,0,0,0)$$
$$\boldsymbol{s}_5=\mathrm{col}(50,-95,\pi,0,0,0),\ \boldsymbol{s}_6=\mathrm{col}(20,-100,\pi,0,0,0)$$

The positions of 7#–8# virtual leaders are respectively represented as follows:

$$\boldsymbol{p}_{7\mathrm{r}}=\mathrm{col}(40-40\sqrt{2}\sin((\theta_7-800)/200-5\pi/8),\ -40-20\sqrt{2}\cos((\theta_7-800)/200-5\pi/8))$$
$$\boldsymbol{p}_{8\mathrm{r}}=\mathrm{col}(40-40\sqrt{2}\sin((\rho_8-800)/100-5\pi/8),\ -40-20\sqrt{2}\cos((\rho_8-800)/100-5\pi/8))$$

The corresponding time-varying deviation signals of 1#–6# USVs are respectively represented as follows:

$$\boldsymbol{p}_{1\mathrm{d}}=\boldsymbol{p}_{2\mathrm{d}}=\boldsymbol{p}_{3\mathrm{d}}=\mathrm{col}(0,0)$$
$$\boldsymbol{p}_{4\mathrm{d}}=\mathrm{col}(25\sin t/50,25\cos t/50)$$
$$\boldsymbol{p}_{5\mathrm{d}}=\mathrm{col}(25\sin(t/50+2\pi/3),25\cos(t/50+2\pi/3))$$
$$\boldsymbol{p}_{6\mathrm{d}}=\mathrm{col}(25\sin(t/50+4\pi/3),25\cos(t/50+4\pi/3))$$

The kinematic parameters of 1#–3# USVs are $\boldsymbol{K}_{ci}$ = diag{0.18, 0.775}, i = 1, 2, 3, δ_{i1} = 5 and ς_i = 2. The kinematic parameters of 4#–6# USVs are $\boldsymbol{K}_{ci}$= diag{0.5, 2}, i = 4, 5, 6, and δ_{i1} = 5.

Considering that all USVs use the same physical model, this paper sets the kinetic parameters at δ_{i2} = 2, δ_{i3} = 2, δ_{i4} = 2, μ^u_{ic} = 2, μ^φ_{ic} = 2, and μ^u_{ic} = 5, and ESO parameters at μ^u_{i1} =20, μ^u_{i2} = 200, μ^φ_{i1} =30, μ^φ_{i2} = 300, and μ^φ_{i3} = 1 000.

Fig.4 shows the simulation results of the time-varying formation system guided by multiple leaders. As can be seen from the figure, the two virtual leaders, 7# and 8#, move along the given parameterized paths $\boldsymbol{p}_{7\mathrm{r}}$ and $\boldsymbol{p}_{8\mathrm{r}}$ to form a circle, respectively. According to the communication topology shown in Fig. 3, 1#–3# USVs converge simultaneously and are eventually evenly distributed between two virtual leaders, keeping in a straight line. 4# USV obtains the central position of the virtual leader and uses it as a formation reference point. 4#–6# USVs, respectively, under the action of given time-varying input signals $\boldsymbol{p}_{4\mathrm{d}}$, $\boldsymbol{p}_{5\mathrm{d}}$, and $\boldsymbol{p}_{6\mathrm{d}}$, with the formation reference point as the center of the circle, rotate clockwise around the reference point in a circle of radius of 25 m, move forward in synergy with the virtual leader, and always maintain the triangular formation shown in Fig. 4.

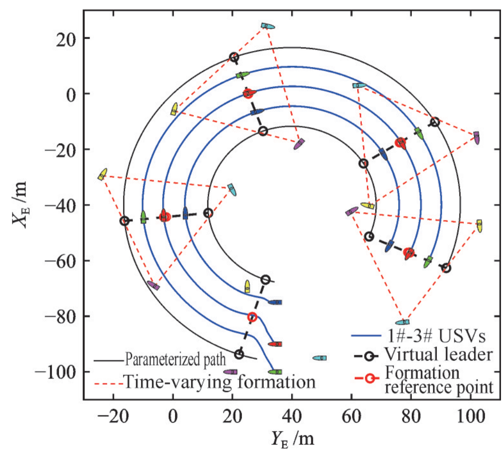

Fig.4 Time-varying formation structure guided by multiple virtual leaders

Fig. 5 and Fig. 6 show that the tracking error of all USVs in the NED reference frame converges to a value within the threshold at steady state and fluctuates up and down in this range. Figs. 7–10 show the actual speed and desired speed of the USV, as well as the actual heading and desired heading curves. It can be seen from the figures that, based on ESO, the surge speed control laws and the yaw rate control laws enable the USV to keep up with the desired value in a short time and keep it moving at the desired value. The physical quantities in each figure are represented as follows: u_1–u_6 are actual speeds; $u_1^*-u_6^*$ are desired speeds (Fig. 7 and Fig. 8); φ_1–φ_6 are actual heading; $\varphi_1^*-\varphi_6^*$ are desired heading (Fig. 9 and Fig. 10).

Fig. 11 and Fig.12 show the control input curves of thrust in the u direction and the control input torque curves in the r direction for all USVs, respec-

downloaded from www.ship-research.com

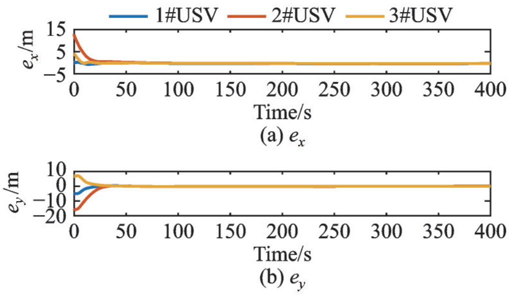

Fig.5 1#–3# USVs' tracking error of the NED reference frame

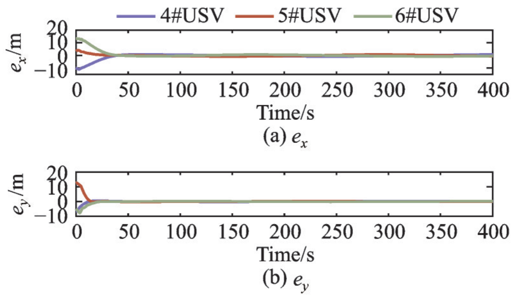

Fig.6 4#–6# USVs' tracking error of the NED reference frame

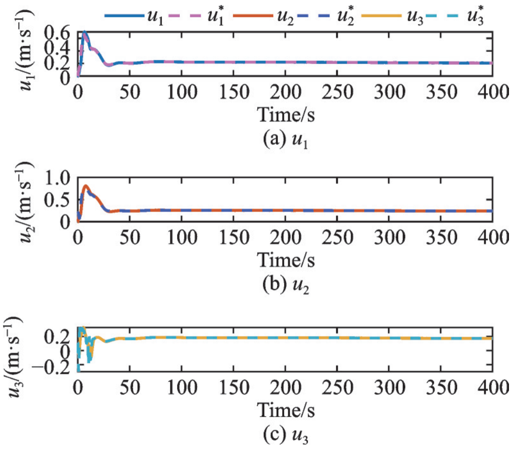

Fig.7 Actual speed and desired speed of 1#–3# USVs

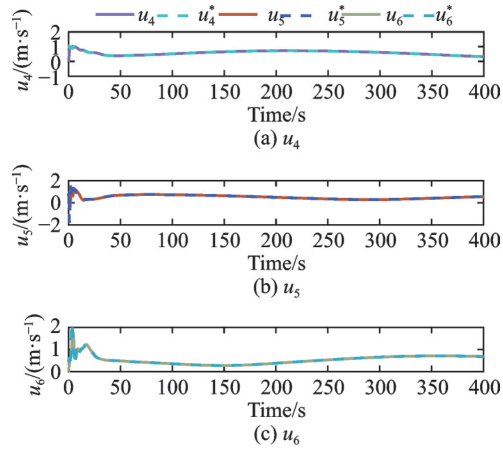

Fig.8 Actual speed and desired speed of 4#–6# USVs

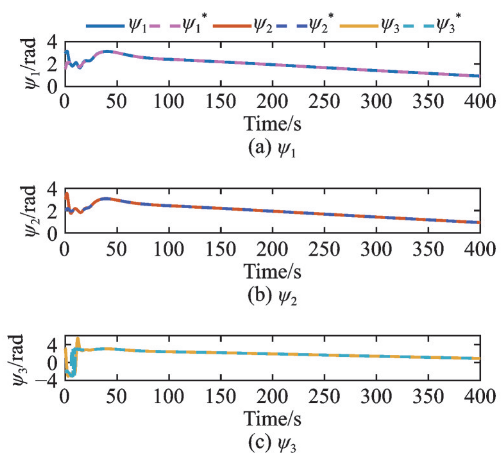

Fig.9 Actual heading and desired heading of 1#–3# USVs

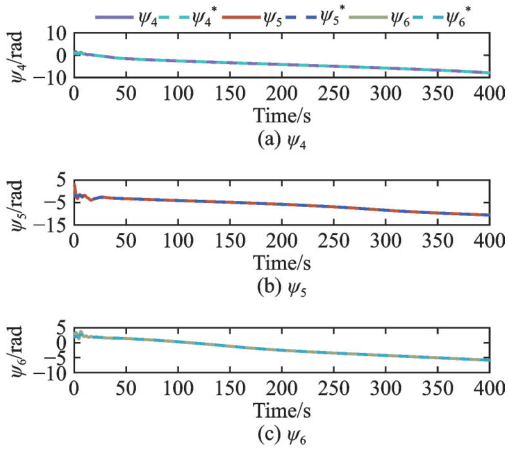

Fig.10 Actual and desired heading of 4#–6# USVs

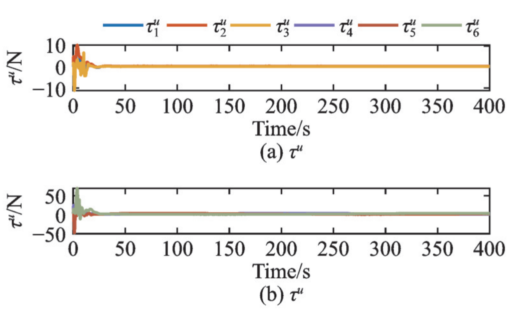

Fig.11 Control input of all USVs' thrust in the u direction

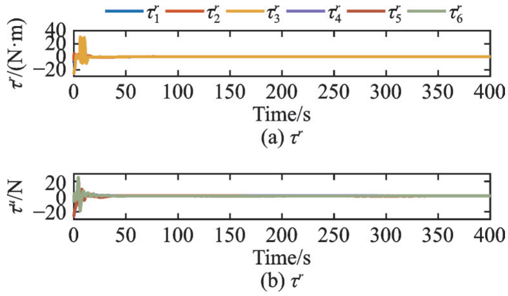

Fig.12 Control input of all USVs' torque in the r direction

tively. Fig. 13 shows the variation curve of path parameters for two virtual leaders. It can be seen by coupling Fig. 4 that because the initial position of the given USV lags behind the virtual leader, in order to realize the synergy between the virtual leader and the USV, we update the path parameters with negative values so that the virtual leader can approach the USV, and when it approaches the USV, the synergistic movement around the circle shown in Fig. 4 begins.

downloaded from www.ship-research.com

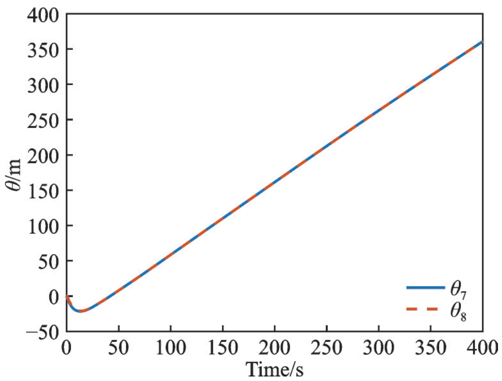

Fig.13 The parameter update curves of virtual leader

5 Conclusions

This paper mainly introduces the issue of distributed time-varying formation control for USVs guided by multiple leaders with model uncertainties and unknown ocean disturbances. Firstly, at the kinematic level, distributed time-varying formation guidance laws are designed on the basis of the containment method, path maneuvering principles, and neighboring information (position, surge speed, and heading). Then, at the kinetic level, the surge speed and yaw rate control laws are developed on the basis of the ESO method to estimate the model uncertainties and unknown ocean disturbances during the navigation of USVs. Further, cascade system stability analysis is undertaken to validate the input status stability of the closed-loop control system for the time-varying formation of USVs, and the effectiveness of this method is demonstrated via simulation.

References

[1] DONG X W, YU B C, SHI Z Y, et al. Time-varying formation control for unmanned aerial vehicles: theories and applications [J]. IEEE Transactions on Control Systems Technology, 2015, 23 (1): 340-348.

[2] JIN K F, WANG H D, YI H, et al. Key technologies and intelligence evolution of maritime UV [J]. Chinese Journal of Ship Research, 2018, 13 (6): 1-8 (in Chinese).

[3] ZHANG X D, LIU S L, LIU Y, et al. Review on development trend of launch and recovery technology for USV [J]. Chinese Journal of Ship Research, 2018, 13 (6): 50-57 (in Chinese).

[4] LIU L, WANG D, PENG Z H. State recovery and disturbance estimation of unmanned surface vehicles based on nonlinear extended state observers [J]. Ocean Engineering, 2019, 171: 625-632.

[5] PARK B S, YOO S J. An error transformation approach for connectivity-preserving and collision-avoiding formation tracking of networked uncertain underactuated surface vessels [J]. IEEE Transactions on Cybernetics, 2019, 49 (8): 2955-2966.

[6] HWANG H G, KIM H W, KIM B S, et al. A development of integrated control system for platform equipments of unmanned surface vehicle (USV) [J]. Journal of the Korea Institute of Information and Communication Engineering, 2017, 21 (8): 1611-1618.

[7] YU Y L, SU R B, FENG X, et al. Tracking control of backstepping adaptive path of unmanned surface vessels based on surge-varying LOS [J]. Chinese Journal of Ship Research, 2019, 14 (3): 163 - 171 (in Chinese).

[8] OH H, NIU H, TSOURDOS A, et al. Development of collision avoidance algorithms for the C-Enduro USV [C]. //Proceedings of the 19th World Congress. Cape Town, South Africa: The International Federation of Automatic Control (IFAC), 2014: 12174-12181.

[9] LONG G Y, WANG M. Fuzzy decoupling constant-velocity navigation control algorithm for dynamic positioning ship [J]. Chinese Journal of Ship Research, 2019, 14 (3): 152-157 (in Chinese).

[10] PENG Z H, WANG J, WANG D. Distributed maneuvering of autonomous surface vehicles based on neuro dynamic optimization and fuzzy approximation [J]. IEEE Transactions on Control Systems Technology, 2018, 26 (3): 1083-109.

[11] DAI S S, HE S D, HAI L, et al. Platoon formation control with prescribed performance guarantees for USVs [J]. IEEE Transactions on Industrial Electronics, 2018, 65 (5): 4237-4246.

[12] LI T S, ZHAO R, FANG L Y, et al. Finite-time formation control of under-actuated ships using nonlinear sliding mode control [J]. IEEE Transactions on Cybernetics, 2018, 48 (11): 3243-3253.

[13] YUAN C Z, LICHT S, HE H B. Formation learning control of multiple autonomous underwater vehicles with heterogeneous nonlinear uncertain dynamics [J]. IEEE Transactions on Cybernetics, 2018, 48 (10): 2920-2934.

[14] BEARD R W, LAWTON J, HADAEGH F Y. A coordination architecture for spacecraft formation control [J]. IEEE Transactions on Control Systems Technology, 2001, 9 (6): 777-790.

[15] KHOSHNAM S. Observer-based neural adaptive formation control of autonomous surface vessels with limited torque [J]. Robotics and Autonomous Systems, 2016, 78: 83-96.

[16] LIU X M, GE S S, GOH C H, et al. Formation potential field for trajectory tracking control of multi-agents in constrained space [J]. International Journal of Control, 2016, 24: 2137-2151.

[17] PENG Z H, GU N, LIU L, et al. Extended state observer design for autonomous surface vehicles using position-yaw measurements [C]. //The 4th International Conference on Information, Cybernetics and Computational Social Systems (ICCSS). Dalian, China: IEEE, 2017.

[18] YU X, LIU L. Distributed formation control of nonholonomic vehicles subject to velocity constraints [J]. IEEE Transactions on Industrial Electronics, 2016, 63 (2): 1289-1298.

[19] MIAO Z Q, LIU Y H, WANG Y N, et al. Distributed estimation and control for leader-following formations of

downloaded from www.ship-research.com

nonholonomic mobile robots [J]. IEEE Transactions on Automation Science and Engineering, 2018, 115 (4): 1946-1954.

[20] DO K D. Formation tracking control of unicycle-type mobile robots with limited sensing ranges [J]. IEEE Transactions on Control Systems Technology, 2008,16 (3): 527-538.

[21] ALMEIDA J, SILVESTRE C, PASCOAL A. Cooperative control of multiple surface vessels in the presence of ocean currents and parametric model uncertainty [J]. International Journal of Robust and Nonlinear Control, 2010, 20: 1549-65.

[22] FUKO T, NAKAGAWA H, ADACHI N. Adaptive tracking control of a nonholonomic mobile robot [J]. IEEE Transactions on Robotics and Automation, 2000, 16 (5): 609-615.

[23] GUO B, WU Z, ZHOU H. Active disturbance rejection control approach to output-feedback stabilization of a class of uncertain nonlinear systems subject to stochastic disturbance [J]. Transactions on Automation Control, 2016, 61 (6): 1613-1618.

[24] LEE S, FUJINO M. Assessment of a mathematical model for the manoeuvring motion of a twin-propeller twin-rudder ship [J]. International Shipbuilding Progress, 2003, 50 (1/2): 109-123.

[25] KHALIL H K. Nonlinear control [M]. Upper Saddle River: Prentice Hall, 2015.

[26] SKJETNE R, FOSSEN T I, KOKOTOVIC P V. Adaptive maneuvering, with experiments for a model ship in a marine control laboratory [J]. Automatica, 2005, 41 (2): 289-298.

多领航者导引无人船集群的分布式时变队形控制

吴文涛，古楠，彭周华*，刘陆，王丹
大连海事大学 船舶电气工程学院，辽宁 大连 116026

摘　要：[**目的**]针对含有模型高度不确定性和未知海洋环境扰动的无人船集群，研究多领航者导引的欠驱动无人船(USV)集群的分布式时变队形控制问题。[**方法**]首先，在运动学层级，基于包含策略和路径操纵原理，设计时变队形分布式制导律；然后，在动力学层级，针对USV航行中存在的模型不确定性以及未知海洋环境扰动，设计基于扩张状态观测器(ESO)的前向速度和艏摇角速度控制律，减小模型不确定性和未知海洋环境扰动带来的影响；最后，进行级联系统稳定性分析和控制器有效性的仿真验证。[**结果**]研究表明，无人船集群采用的分布式时变编队闭环控制系统输入状态稳定，仿真结果证明了控制方法的有效性。[**结论**]所提出的控制器可以使无人船集群形成预定的时变编队队形，并跟踪多领航者形成的凸包。

关键词：欠驱动无人船；制导和控制律；时变队形控制；多领航者；扩张状态观测器

[*Continued from page* 9]

多UUV搜索海底声信标任务规划方法

张宏瀚*，郭焱阳，许亚杰，李本银，严浙平
哈尔滨工程大学 自动化学院，黑龙江 哈尔滨 150001

摘　要：[**目的**]为了提高特定海域内多水下无人航行器(UUV)执行海底声信标搜索任务时的搜索性能，需增加对目标的搜索概率。[**方法**]首先，给出各UUV所载被动声呐的搜索能力指标函数，采用蒙特卡罗方法模拟海底声信标的坐标位置，并在任务区域建立搜索能力函数，从而得到本次优化任务的优化目标；然后，根据UUV实际执行任务时的队形要求建立本次优化的约束条件，整合得到基于海底声信标搜索概率最大化的多UUV队形优化模型，并使多UUV按照此队形完成指定区域的声信标搜索工作；最后，采用遗传算法对优化模型进行参数优化，通过设定合理的目标函数以及改进传统的遗传算子使目标函数的值达到设定标准，随之取出相应的参数完成值的选择。[**结果**]将求解出的优化队形与传统优化队形进行对比发现，求解出的优化队形具有更高的发现海底信标的平均概率。[**结论**]该方法能够有效提升多UUV对海底声信标的搜索性能，并给出合理的队形优化方案。

关键词：多水下无人航行器；队形优化；搜索概率；遗传算法

downloaded from www.ship-research.com